JOURNAL OF SOLID STATE CHEMISTRY 75, 313–331 (1988)

Bonding and Stability of the Cr^+ Ion in Octahedral Fluoride Lattices: Results of Approximate Hartree–Fock–Roothaan Calculations

G. FERNANDEZ RODRIGO AND L. PUEYO

Departamento de Química Física y Analítica, Facultad de Química, Universidad de Oviedo, 33007 Oviedo, Spain

Received March 11, 1987; in revised form February 8, 1988

Frozen-core Hartree–Fock–Roothaan calculations at several values of the metal–fluoride distance have been performed for the $(CrF_6)^{5-}$ cluster in an attempt to study the stability of the Cr^+–F^- bond in fluoride lattices. The separate effects on the $^6A_{1g}$ ground state of the $3d$ basis set and the type of core-valence partition have been analyzed. Whereas inclusion of the $3s$ and $3p$ metallic AO's in the valence shell seems to be unnecessary for obtaining a stable cluster ground state, the diffuse $4s$ and $4p$ AO's play a significant role in describing the equilibrium geometry of this complex ion. The metal–ligand covalency is examined and related to the information deduced from the curvature of the $^6A_{1g}$ nuclear potential and the orbital energies of the valence MO's. Consideration of the point-charge lattice potential of the NaF leaves the cluster electron density almost unchanged but noticeably decreases the cluster valence energy. It also reduces the size of the cluster by nearly 0.2 Å. As an alternative stabilizing mechanism, a ligand-to-lattice charge transfer has been explored. At the cluster-*in-vacuo* level it produces electron-deficient clusters more stable than the $(CrF_6)^{5-}$ unit. As an example, the $^7T_{1u}$ state of the neutral CrF_6 cluster (a system in which the oxidation state of the metal is nominally +1) has been computed and compared with the $^6A_{1g}$ state. This CrF_6 unit turns out to be smaller and more strongly bonded than the $(CrF_6)^{5-}$ ion but the latter becomes more stable when the point-charge potential of the NaF is taken into account.

I. Introduction

The Cr^+ ion has been detected in Cr^{2+}-doped crystals after X-ray irradiation (*1–11*). The Cr^{2+} ion behaves as an efficient electron trap due to its trend to reach the d^5 configuration. Octahedral (*1–4*) and cubal (*5–7*) coordinations of fluorides around the Cr^+ ion have been detected by EPR and ENDOR spectroscopies. Cr^+ centers in fluoride compounds are stable for hours or days depending on the manner the sample is conserved (*1*).

The available experimental information on these centers is very scarce, being essentially limited to magnetic resonance data. For instance, their optical spectra are unknown due to low Cr^+ concentrations and the weakness of the d–d electronic transitions within the d^5 configuration. Details of the geometry and electronic structure of the Cr^+ centers are also unknown. Metal–ligand equilibrium distances determined from superhyperfine parameters (*12, 13*) are, as far as we know, the only structural information available. These determinations give $R_e(Cr^+–F^-) = 2.47 \pm 0.02$ Å for $Cr^+ : NaF$ and 2.35 ± 0.02 Å for $Cr^+ : KMgF_3$ (*14*).

From the computational side, the avail-

0022-4596/88 $3.00

able information is also scarce. The octahedral $(CrF_6)^{5-}$ cluster *in vacuo* has been considered by some workers as a model for the interpretation of the superhyperfine parameters of the Cr^+ centers. Clack *et al.* (*15, 16*) reported INDO and CNDO calculations on this cluster directed to the determination of transferred spin densities. Larsson (*17*) performed a multiple-scattering $X\alpha$ calculation in connection with the same problem. Our own group briefly referred to the $(CrF_6)^{5-}$ cluster in a recent report on the calculation of equilibrium geometries of transition-metal ions in ionic fluorides (*18, 19*).

In this work we present the results of a theoretical investigation (*20*) on Cr^+ centers in fluorides based on frozen-core (FC) Hartree–Fock–Roothaan (HFR) cluster calculations. We analyze the electronic structure of the $(CrF_6)^{5-}$ cluster *in vacuo* and in the point-charge potential of the NaF crystal at several values of the chromium–fluoride distance along the a_{1g} vibration of the octahedral cluster. In the analysis of the potential curve of the $^6A_{1g}$ cluster ground state, we discuss the importance of the quality of the 3*d* basis, the influence of size and type of the valence shell adopted in the calculation, the role of the diffuse 4*s* and 4*p* AO's, and the contributions of the external lattice potential. From the self-consistent-field (SCF) solutions of the $^6A_{1g}$ state at several values of R, we study the R dependence of the metal–fluoride covalency, spin transfer, and electron delocalization.

Our results reveal the difficulties encountered in the theoretical determination of the geometry and stability of a monopositive ion as the Cr^+ in an octahedral site by means of a cluster model. Although our cluster-*in-vacuo* calculations give a reasonable ground state nuclear potential and an equilibrium metal–ligand distances consistent with the values deduced from magnetic resonance data, the idea of describing the Cr^+ center in terms of a cluster-*in-vacuo* calculation of this sort is probably inadequate, given the important direct lattice effects on the cluster ground state. Larger cluster sizes and more elaborate lattice models would probably be required in order to reach full confidence in the nonempirical prediction of the geometry of these monopositive centers.

The theoretical description of the covalency and spin density of the center presents some difficulties also. Our results show that the ligand-to-metal (L–M) charge transfer determined by means of Mulliken population analysis is unphysically large. This is because the 4*s* and 4*p* AO's required for a satisfactory description of the cluster wavefunction extend largely into the ligand sites. Under these circumstances, the equipartition of the overlap charge density proposed by Mulliken is clearly inadequate. Many alternatives to this partition have been proposed but, unfortunately, a nonarbitrary population analysis seems to be inexistent. This means that more research will be required before having an accurate description of the electron delocalization in these 3*d* systems.

This last question led us to consider an alternative mechanism for analyzing the electron delocalization in the hexafluoride cluster. We have explored an isotropic ligand-to-lattice (LLAT) charge transfer which gives rise to cluster-deficient systems. Particular attention has been paid to the neutral CrF_6 unit, which can be considered as an alternative cluster-*in-vacuo* approach to the Cr^+-containing fluorides. Our calculations indicate that the LLAT charge transfer makes the CrF_6 unit smaller and more tightly bonded than the $(CrF_6)^{5-}$ system. Furthermore, the lower ligand electron occupation of this cluster reduces the direct lattice effects and the difficulties encountered within Mulliken analysis. The cluster-*in-vacuo* predictions deduced from this unit are very slightly modified by the action of the corresponding potential of the

TABLE I

METAL AND LIGAND STO BASIS SETS (REFS. *22–24*)

A. Metallic basis sets

AO\STO	1*s*(23.39)	2*s*(8.9)	3*s*(4.06)	4*s*(1.75)
$1s_M$	1.0			
$2s_M$	−0.36240564	1.06364368		
$3s_M$	0.14156036	−0.47925202	1.09703726	
$4s_M$	−0.04246753	0.14647754	−0.38365720	1.05957517

AO\STO	2*p*(9.70)	3*p*(3.74)	4*p*(1.48)
$2p_M$	1.0		
$3p_M$	−0.30745939	1.04619852	
$4p_M$	0.07726496	−0.28882147	1.03743504

$3d_M(Cr^+)$:	0.67472273(1.80)	+ 0.50579215(4.95)
$3d_M(Cr^{3+})$:	0.58216579(2.20)	+ 0.54596792(4.95)

B. Fluoride basis set

AO\STO	2*s*(8.7)	2*s*(2.425)	AO\STO	2*p*(2.425)
$1s_F$	1.0		$2p_F$	1.0
$2s_F$	−0.21754530	1.02338944		

electron-rich external lattice. These results suggest that the LLAT mechanism briefly presented in this paper could be an interesting scheme for studying highly charged complex ions at the cluster-*in-vacuo* level since the resulting electron-deficient units may reveal, without expensive calculations, some of the features of the nominal cluster-lattice-system.

In the next section we present our results on the geometry of the Cr^+ center. Section III is dedicated to the covalency and L–M charge transfer, and the last section to the discussion of the LLAT scheme.

II. Ground State Nuclear Potential and Orbital Energies of $(CrF_6)^{5-}$

We have used the open-shell FC HFR methodology of Richardson *et al.* (*21*) and the Slater-type-orbital (STO) basis sets of Refs. (*22*) and (*23*) (Table I). The STO fluoride basis has been taken from Ref. (*24*). In combination with these STO basis sets, this approximate HFR methodology has given very accurate results in the calculation of different observables for analogous systems. We can mention the spectral calculations on $(NiF_6)^{4-}$ (*24*), $(CrF_6)^{3-}$ (*25*), $(CrF_6)^{4-}$ (*26*), $(CrF_6)^{2-}$ (*27*), and $(MnF_6)^{4-}$ (*28*); the bonding and electronic structure calculations on $(Co(NH_3)_6)^{3+}$ (*29*) and $(NiF_6)^{4-}$ (*24*, *30*), and the analysis of the cluster–lattice interaction in several chromium fluorides (*31*).

Here we are interested in the theoretical description of the ground state of the $(CrF_6)^{5-}$ unit and, in particular, in the following questions:

(a) the importance of the 3*d* basis in the shape of the ground state curve;

(b) the relative contributions of different valence AO's to the Cr^+–F^- bond;

(c) the role of the core-valence orthogonality;

(d) the significance of the external lattice potential.

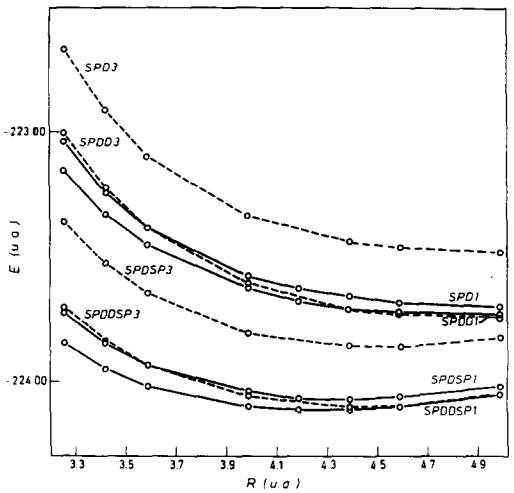

FIG. 1. Potential energy curves for different definitions of the valence shell according to unprojected (U) calculations. Numbers 1 and 3 stand for Cr^{+} (solid lines) and Cr^{3+} (broken lines) bases, respectively.

Thus, in the present calculation we have considered different $3d$ functions, several definitions of the valence shell, core-projection operators that improve the required core-valence orthogonality, and the point-charge lattice potential of the NaF crystal. The $3d$ AO's considered in this work are the nominal Cr^{+} wavefunction and the Cr^{3+} AO of Ref. (*22*). The following core-valence partitions have been examined:

Partition name	Metallic AO's in the valence shell
SPD	$3s_M$, $3p_M$, $3d_M$
SPDD	$3s_M$, $3p_M$, $3d_M$, $3d_i$
DDSP	$3d_M$, $3d_i$, $4s_M$, $4p_M$
SPDSP	$3s_M$, $3p_M$, $3d_M$, $4s_M$, $4p_M$
SPDDSP	$3s_M$, $3p_M$, $3d_M$, $3d_i$, $4s_M$, $4p_M$

where the $3d_i$ AO is the inner STO of the 2ζ $3d_M$ function in Table I. In all these partitions the ligand valence shell includes the $2s_F$ and $2p_F$ AO's of the six fluoride ions.

Within these five partitions and using the two representations of the $3d$ AO's we have solved the FC HFR equations corresponding to the ${}^6A_{1g}$ ground state of the $(CrF_6)^{5-}$ cluster at several values of R.

Let us see first the cluster-*in-vacuo* results. Basis and partition effects can be appreciated in Fig. 1. The information collected in this figure has been obtained with the methodology as described in Ref. (*21*), i.e., without core-projection operators in the Fock Hamiltonian. We will refer to this type of results as U or unprojected results.

From Fig. 1 we observe that the diffuse $4s$ and $4p$ AO's are necessary to obtain a stable ground state. We find R_e(SPDSP) = 2.30 Å and R_e(SPDDSP) = 2.55 Å with the Cr^{+} $3d$ basis and R_e(SPDSP) = 2.36 Å and R_e(SPDDSP) = 2.32 Å with the Cr^{3+} basis. As expected, the former basis is more efficient from the variational point of view: for a given partition it gives valence energies some 8 eV below those obtained with the Cr^{3+} basis. As a consequence, calculations involving two $3d$ AO's (DD) give larger improvements over the D results for the Cr^{3+} basis, showing that the efficiency of an extra function in the active space is smaller for better optimized sets. This effect is independent of the presence of the $4s$ and $4p$ functions, indicating independent variational effects in different blocks of symmetry. Inclusion of these diffuse functions in the SCF process is variationally more efficient than the D → DD extension.

Comparing these results with those obtained for other oxidation states of chromium reveals that $(CrF_6)^{5-}$ is the only system having a SPDD nuclear potential without minimum. This suggests that the theoretical description of the equilibrium properties of ML_6 transition-metal clusters is probably a more difficult task for large and polarizable monopositive ions than for the relatively smaller and less polarizable di- or tripositive cations.

Let us now discuss the effects of the core projection in the shape of the nuclear potential. This projection is a remedy to the problem of the insufficient core-valence orthogonality in FC calculations (*32–34*). It has been discussed recently (*18, 35*) in con-

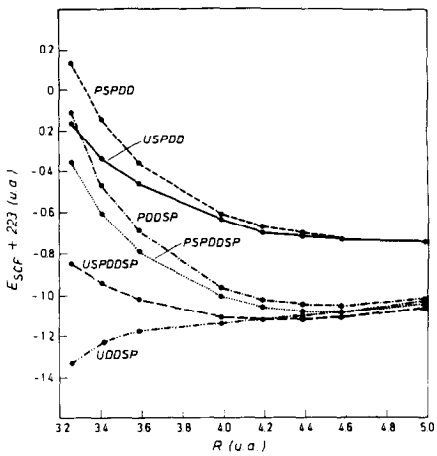

FIG. 2. Core-projection effects on the ground-state nuclear potentials of the $(CrF_6)^{5-}$ cluster.

nection with the methodology of Richardson *et al.* (*21*). Luaña *et al.* (*18*) refer to the $(CrF_6)^{5-}$ system in comparison with other chromium hexafluorides. We will add here a few comments on some important results of the core projection in this cluster.

In Fig. 2 we show the SPDD, DDSP, and SPDDSP nuclear potentials of the $^1A_{1g}$ ground state computed with and without core projection. From this figure we deduce that:

(i) Lack of minimum in the U-DDSP nuclear potential is not due to freezing of the $3s_M$ and $3p_M$ AO's into the core since the P-DDSP results show a minimum. The problem with the U-DDSP basis is clearly the nonorthogonality of the $3s_M$ and $3p_M$ AO's with the $2s_F$ and $2p_F$ valence AO's (*18*).

(ii) Lack of minimum in the U-SPDD partition cannot be attributed to insufficient core-valence orthogonality since the P-SPDD potential does not show it either. A lack of diffuse functions seems to be the reason for these continuously repulsive SPDD nuclear potentials.

(iii) U-SPDSP and U-SPDDSP potentials present energy minima due, apparently, to the action of the diffuse functions. Insufficient core-valence orthogonality is not here as severe as it is in the DDSP partition but it still produces inward shifts of 0.07 Å (SPDSP) and 0.12 Å (SPDDSP).

(iv) P-DDSP and P-SPDDSP calculations give R_e = 2.375 Å, showing the importance of the diffuse functions in computing the ground state. According to this, the presence of the $3s_M$ and $3p_M$ AO's in the valence shell seems to be uncessary for having a stable ground state in $(CrF_6)^{5-}$. This result has also been found in other chromium clusters (*18*).

At this point, it should be emphasized that from a conceptual point of view the P-SPDDSP partition is the best one, among all considered here, because it contains the largest valence space and the core-projection refinement. All other calculations discussed in this work illustrate several contributions from different AO's or different approximations but they are, in principle, inferior to the P-SPDDSP one. In consequence, the P-SPDDSP value for R_e (2.375 Å) should be considered as our best prediction from the present cluster-*in-vacuo* calculation. This value is slightly smaller than the 2.417 Å obtained if the renormalization correction discussed by Kalman and Richardson (*29*) is taken into account (*19*). Both renormalized and unrenormalized values are consistent with those deduced from the observed superhyperfine constant A_s (*14*): 2.47 Å for Cr^+ : NaF and 2.34 Å for Cr^+ : $KMgF_3$.

Let us now comment briefly on the behavior of the orbital energies of the valence MO's. In Table II we collect U-SPDDSP and P-SPDDSP values computed at several distances. We can observe that the effects of the core projection on these energies are negligible. These orbital energies are decreasing functions of the metal–ligand distance R. They group together according to the dominant AO in their corresponding MO, revealing a weak mixture among metal

TABLE II

ORBITAL ENERGIES (HARTREE) OF THE VALENCE MO'S FROM THE SPDDPS CALCULATIONS ON THE $^6A_{1g}$ GROUND STATE OF THE $(CrF_6)^{5-}$ CLUSTER

	R (Bohr)					
	3.59	3.99	4.19	4.39	4.59	4.99
$1a_{1g}(3s_M)$	−1.6794	−1.8725	−1.9579	−2.0361	−2.1077	−2.2339
	−1.6899	−1.8858	−1.9697	−2.0459	−2.1155	−2.2385
$2a_{1g}(2s_F)$	−0.1901	−0.2448	−0.2694	−0.2921	−0.3131	−0.3499
	−0.1726	−0.2360	−0.2630	−0.2874	−0.3096	−0.3480
$3a_{1g}(2p\sigma_F)$	0.7247	0.6799	0.6610	0.6437	0.6278	0.6002
	0.7516	0.6908	0.6680	0.6482	0.6307	0.6015
$1t_{1u}(3p_M)$	−0.5208	−0.7029	−0.7864	−0.8635	−0.9346	−1.0606
	−0.5320	−0.7166	−0.7985	−0.8736	−0.9426	−1.0635
$2t_{1u}(2s_F)$	−0.1877	−0.2461	−0.2708	−0.2934	−0.3142	−0.3507
	−0.1715	−0.2373	−0.2643	−0.2886	−0.3107	−0.3488
$3t_{1u}(2p\sigma_F)$	0.7312	0.6884	0.6688	0.6506	0.6339	0.6047
	0.7597	0.7024	0.6787	0.6576	0.6388	0.6071
$4t_{1u}(2p\pi_F)$	0.7875	0.7353	0.7103	0.6868	0.6650	0.6273
	0.8003	0.7418	0.7152	0.6905	0.6679	0.6289
$1e_g(2s_F)$	−0.1993	−0.2472	−0.2704	−0.2925	−0.3131	−0.3496
	−0.1823	−0.2384	−0.2640	−0.2878	−0.3096	−0.3478
$2e_g(2p\sigma_F)$	0.7538	0.7238	0.7059	0.6878	0.6702	0.6374
	0.7651	0.7269	0.7075	0.6887	0.6707	0.6377
$3e_g(3d_e)$	1.2547	1.0507	0.9622	0.8813	0.8071	0.6755
	1.2698	1.0467	0.9562	0.8751	0.8015	0.6717
$1t_{2g}(2p\pi_F)$	0.7647	0.7148	0.6918	0.6706	0.6511	0.6177
	0.7793	0.7233	0.6984	0.6756	0.6549	0.6198
$2t_{2g}(3d_t)$	1.2082	1.0127	0.9282	0.8511	0.7805	0.6559
	1.1958	0.9995	0.9167	0.8416	0.7730	0.6514
$1t_{1g}(2p\pi_F)$	0.7750	0.7210	0.6965	0.6739	0.6535	0.6189
	0.7915	0.7303	0.7035	0.6792	0.6575	0.6210
$1t_{2u}(2p\pi_F)$	0.7767	0.7218	0.6970	0.6743	0.6538	0.6190
	0.7931	0.7311	0.7040	0.6796	0.6577	0.6211

Note. First and second row correspond to unprojected and projected calculations, respectively.

and ligand functions in this cluster. This result may be related to the weak bonding interaction suggested by the very shallow nuclear potential of the $^6A_{1g}$ state seen in Fig. 1. At any value of R, the ordering of these orbital energies turns out to be:

$$\varepsilon(3s_M) < \varepsilon(3p_M) < \varepsilon(2s_F) < \varepsilon(2p_F) < \varepsilon(3dt_{2g}) < \varepsilon(3de_g).$$

The splitting of the $2s_F$ states ($2a_{1g}$, $2t_{1u}$, and $1e_g$) is negligibly small at any distance. That of the $2p_F$ states is a little greater. Both increase when R decreases, as expected. Thus, we see that the metal–$2s_F$ interaction is very weak, weaker than the metal–$2p_F$ one. The $3d$ splitting in $3dt_{2g}$ and $3de_g$ is clearly visible and decreases when R increases. By comparing orbital energies obtained in different partitions we can see that the D → DD extension produces a very slight reduction in all of them. This change is, in absolute value, smaller than those due to the addition of the diffuse functions. The $4s$ and $4p$ AO's reduce the orbital energies

of the bonding orbitals and increase those of the antibonding ones, making more bonding the bonding MO's and more antibonding the antibonding MO's. This means larger metal–ligand bonding interactions. We observe again that the diffuse functions contribute significantly to make stronger the Cr^+–F^- bond.

The cluster-*in-vacuo* calculations have been complemented with a calculation of the $(CrF_6)^{5-}$ unit in the electrostatic potential of the NaF crystal. The lattice of the NaF has been approximated by a network of point charges located at the crystallographic sites. The electrostatic potential has been calculated by the Eward method (*36*) at many points inside a sphere of radius 5 Bohr centered at the metal site. These values are then represented by an accurate one-electron operator containing 17 fitting parameters and defined as a linear combination of a_{1g} functions. This operator simulates the Ewald potential with deviations smaller than 0.7 mhartree. It is incorporated into the cluster Fock operator before the SCF process. For brevity, we will refer only to the P-SPDDSP case, although we found qualitatively analogous results for other partitions.

In Table III we present P-SPDDSP valence energies for the $(CrF_6)^{5-}$ unit *in vacuo* and in the electrostatic potential of the NaF. This lattice potential produces a cluster stabilization of about 4.6 hartree (125 eV) and reduces the cluster-*in-vacuo* value of R_e from 2.375 to 2.194 Å. A reduction in the cluster-*in-vacuo* R_e should be anticipated since this value is larger than the Na^+–F^- distance in the pure NaF (2.317 Å). Thus, the $(CrF_6)^{5-}$ cluster should shrink a little bit in order to fit the NaF lattice.

On the other hand, both the present cluster-*in-vacuo* results and the values of R_e obtained from the A_s constant (*14*) suggest that the Cr^+ ion has an ionic radius slightly larger than the Na^+ ion. This should tend to produce a small outward fluoride relaxation in NaF upon Cr^+ substitution. In other words, our cluster-in-the-lattice value of R_e could be expected to be slightly larger than the value of the pure host. We obtained, however, a value of R_e noticeably smaller than 2.317 Å, possibly due to the crude approximation of the point charges as well as to the total neglect of next-nearest-neighbor relaxations.

In our recent theoretical study of 3*d* ions in cubic fluoroperovskites (*19*) we reported effects of the cluster–lattice interaction on the equilibrium metal–ligand distances in terms of a sophisticated (and very expensive) quantum lattice model that includes coulombic, exchange, and lattice projection operators. We obtained $R_e(Cr^+–F^-)$ = 2.198 Å for $Cr^+ : KMgF_3$. Again, this reduction from the cluster-*in-vacuo* value is possibly too large due to lack of relaxation of the next-nearest neighbors. Although the coincidence with the present value for Cr^+ : NaF deduced from a point-charge lattice is clearly accidential, both calculations tell us that the cluster-*in-vacuo* size of the

TABLE III

P-SPDDSP VALENCE ENERGIES (HARTREE), PLUS 224 HARTREES, OF THE $(CrF_6)^{5-}$ UNIT *in Vacuo* AND INSIDE THE POINT-CHARGE POTENTIAL OF THE NaF

	R (Bohr)					
	3.59	3.99	4.19	4.39	4.59	4.99
In vacuo	0.21327	−0.00430	−0.04932	−0.06871	−0.06959	−0.03441
In NaF	−4.51022	−4.69121	−4.70140	−4.67664	−4.62313	−4.43506

$(CrF_6)^{5-}$ unit would be reduced by the cluster lattice interaction. According to the distances obtained from the A_s constant (*14*), the cluster-in-the-lattice values obtained here and in Ref. (*19*) are both too low, in contrast with the situation found for dispositive cations (*19*). It appears that the nonempirical determination of the equilibrium geometry of a monopositive center in terms of a cluster model would possibly require the consideration of a cluster larger than the ML_6 unit and a sophisticated lattice model.

III. Covalency and Ligand–Metal Charge Transfer

We will now explore the predictions of our calculations on the metal–ligand covalency and charge transfer, i.e., on the bonding characteristics of the Cr^+ ion in an octahedral environment of fluorides. The analysis of the covalency will be made in two separate parts. First, we will study the nonclassical energy component of the SCF energy, its R dependence, and the effects of the core projection on such quantity. Since the nonclassical energy can be understood as a direct measure of the metal–ligand quantum–mechanical interaction, we compare it with the mixing of the metal and ligand functions. Second, we will discuss the covalency as deduced from the SCF mixing coefficients and Mulliken population analysis.

In order to compute the nonclassical energy, $E_{nc}(R)$, we can write the SCF valence energy as the sum,

$$E_{SCF}(R) = E(\infty) + \alpha/R + E_{nc}(R) = E_{class}(R) + E_{nc}(R), \quad (1)$$

where $E(\infty) + \alpha/R$ is the classical electrostatic intracluster interaction. $E(\infty)$ is the energy at $R = \infty$ and α can be written as

$$\alpha = 6q_M q_L + (6 \cdot (2)^{1/2} + 3/2)q_L^2, \quad (2)$$

where q_M and q_L are the classical point charges representing the metal and ligand ions of the cluster, respectively. For hexafluorides of monopositive cations as the $(CrF_6)^{5-}$, $q_M = -q_L = 1$ and $\alpha = 3.98528$. A positive α represents a net repulsive interaction among the components of the cluster. On the other hand, α becomes -2.01472 and -8.01472 for the hexafluorides of dipositive and tripositive cations, respectively. The $(CrF_6)^{5-}$ cluster is then a repulsive unit in the classical limit. By contrast with other chromium hexafluorides, the possibly stability of this system must come from purely quantum effects.

In Table IV we present the DDSP, SPDD, and SPDDSP nonclassical energies and the values of $E(\infty)$. $E(\infty)$ is the same for U and P calculations within a given partition because the expectation values of the core-projection operators are zero in the atomic basis set.

In this table we observe that the nonclassical energy is positive for those partitions lacking diffuse functions. Positive nonclassical energies mean that if the cluster is repulsive in the classical approximation the repulsion is still larger in the quantum–mechanical description. In these cases $E_{nc}(R)$ increases with R because the SCF energy goes up at large distances but the classical energy is a continuous decreasing function of R. SCF energies above the classical limit might indicate a poor basis set. However, we did not find such results in our calculations on the $(CrF_6)^{z-}$ ($z = 2$, 3, and 4) systems (*18*). Thus, basis sets of Refs. (*22*) and (*23*) could be somewhat less adequate for Cr^+ than for higher oxidized chromium ions.

Addition of the diffuse $4s_M$ and $4p_M$ functions reduce the SCF energies by amounts large enough to give negative nonclassical energies, as can be seen in Table IV. Notice the great similarity between P-DDSP and P-SPDDSP results. These nonclassical ener-

TABLE IV

NONCLASSICAL ENERGY AND $E(\infty)$ (HARTREE) FOR DIFFERENT CORE-VALENCE PARTITIONS OF THE $(CrF_6)^{5-}$ UNIT

	R (Bohr)				
Partition	3.99	4.19	4.39	4.59	4.99
U-SPDD	0.07043	0.07370	0.08902	0.11226	0.17266
P-SPDD	0.10549	0.09382	0.10059	0.11888	0.17482
U-SPDDSP	−0.36412	−0.32863	−0.28306	−0.22999	−0.10914
P-SPDDSP	−0.26701	−0.26435	−0.24041	−0.20173	−0.09695
U-DDSP	−0.42109	−0.35974	−0.30004	−0.23927	−0.11209
P-DDSP	−0.26109	−0.26423	−0.24236	−0.20393	−0.09842
$E(\infty)$ + 224 hartrees		SPDD	DDSP	SPDDSP	
		−0.70315	−0.70315	−0.73611	

gies suggest that the $3s_M$ and $3p_M$ AO's play a small role in determining the meal–ligand covalency in this cluster. Core projection, as an orthogonality correction, raises the SCF energy and reduces $E_{nc}(R)$. This effect is larger in the DDSP partition. The large values of the U-DDSP nonclassical energy at shorter distances are due to the collapse of the valence shell into the core and do not represent a bonding effect (*18*).

We will return to $E_{nc}(R)$ in the next section in connection with the ligand-to-lattice charge transfer. We conclude this discussion by noticing that P-DDSP and P-SPDDSP nonclassical energies almost coincide.

The contribution of different AO's to the Cr^+–F^- covalency can better be deduced from the analysis of the valence charge distribution. As an example, we present in Table V the cluster-*in-vacuo*, P-SPDDSP SCF coefficients of the mainly metallic MO's obtained at five values of R. The effects of the lattice potential on the cluster charge distribution are too small to alter the following discussion. These P-SPDDSP coefficients are nearly equal to the P-DDSP ones (not shown in the table) confirming the small contribution of the $3s_M$ and $3p_M$ metallic AO's to the covalency. The structure of the mainly $4s_M$, $4a_{1g}$ MO reveals an intense metal–ligand mixing through the $2s_F$ and $2p\sigma_F$ channels. The relative contribution of the latter is comparatively larger when R increases. An analogous picture is deduced from the $5t_{1u}$ MO where the $2p\sigma_F$ AO is again the more efficient channel for the charge transfer, particularly at larger distances.

In Table VI we present the results of Mulliken population analysis at five values of R, as deduced from the P-SPDDSP solutions of the ground state. According to this analysis, the $3s_M$ and $3p_M$ AO's have practically the nominal occupations. The $3d$ AO's receive 0.08–0.20 electrons from the ligands, depending on the value of R. The transfer through the e_g (σ) channel is more than twice the t_{2g} (π) value.

The results corresponding to the $4s_M$ and $4p_M$ AO's deserve separate comment. These functions receive about 0.3 and 0.7 electrons from the ligands, respectively. Thus, a whole electron is transferred through the diffuse AO's according to this analysis. In total, the charge transfer turns out to be 1.02 electrons at R = 4.99 Bohr (2.64 Å) and 1.33 electrons at 3.99 Bohr

TABLE V

SCF COEFFICIENTS OF THE MAINLY METAL MO'S AT SEVERAL METAL–LIGAND DISTANCES: P-SPDDSP CALCULATIONS ON THE $^6A_{1g}$ STATE OF THE $(CrF_6)^{5-}$ CLUSTER

		R (Bohr)				
MO	SAO[a]	3.99	4.19	4.39	4.59	4.99
$4a_{1g}$	$3s_M$	−0.00553	0.00761	0.01573	0.02076	0.02582
	$4s_M$	−1.10919	−1.06328	−1.02949	−1.00494	−0.97544
	χ_s	0.48270	0.40267	0.33772	0.28420	0.20205
	χ_σ	0.60432	0.57426	0.54560	0.51807	0.46590
$5t_{1u}$	$3p_M$	0.01566	0.02722	0.03472	0.03951	0.04436
	$4p_M$	−1.15179	−1.11211	−1.07983	−1.05402	−1.01813
	χ_s	0.53596	0.46767	0.40771	0.35512	0.26846
	χ_σ	0.44974	0.44692	0.43889	0.42705	0.39589
	χ_π	0.29955	0.25692	0.22107	0.19093	0.14405
$3e_g$	$3d_M$	1.02962	1.02255	1.01871	1.01723	1.01833
	$3d_i$	−0.00358	−0.00786	−0.01236	−0.01682	−0.02469
	χ_s	−0.21404	−0.17927	−0.14968	−0.12451	−0.08503
	χ_σ	−0.31217	−0.28630	−0.26080	−0.23590	−0.18885
$2t_{2g}$	$3d_M$	1.06623	1.05792	1.05176	1.04713	1.04085
	$3d_i$	−0.08364	−0.07413	−0.06675	−0.06098	−0.05283
	χ_π	−0.18315	−0.15062	−0.12365	−0.10133	−0.06776

[a] Symmetry-adapted orbital.

(2.11 Å). Such transfer gives rise to a negative chromium ion in the equilibrium region, as can be seen at the bottom of Table VI where we present the metal and ligand charges deduced from Mulliken analysis. Substitution of these charges in Eq. (2)

TABLE VI

ORBITAL POPULATIONS AND METAL AND LIGAND CHARGES ACCORDING TO MULLIKEN POPULATION ANALYSIS: P-SPDDSP CALCULATION ON THE $^6A_{1g}$ STATE OF THE $(CrF_6)^{5-}$ CLUSTER

	R (Bohr)				
AO	3.99	4.19	4.39	4.59	4.99
$3s_M$	2.000	2.000	1.999	1.999	1.999
$4s_M$	0.368	0.362	0.353	0.340	0.307
$3p_M$	5.996	5.993	5.990	5.989	5.987
$4p_M$	0.761	0.748	0.731	0.708	0.646
$3d_e$	2.134	2.124	2.111	2.095	2.066
$3d_t$	3.070	3.050	3.035	3.025	3.012
$3d$ (total)	5.204	5.174	5.146	5.120	5.078
$2s_F$	1.985	1.987	1.989	1.990	1.992
$2p_F$	5.793	5.800	5.808	5.817	5.838
q(Cr)	−0.329	−0.276	−0.219	−0.156	−0.017
q(F)	−0.779	−0.787	−0.797	−0.807	−0.831
α	7.587	7.494	7.389	7.265	6.971

gives the values of the constant α appearing in the last row of Table VI. Thus, the point-charge cluster deducible from Mulliken's analysis is much more repulsive than the nominal unit.

This unphysically large transfer through the diffuse AO's is an artifact of Mulliken's equipartition of the metal–ligand overlap population. This is so because the diffuse functions have appreciable density in the ligand region and their overlap population with the $2s$ and $2p$ ligand functions very much resembles the corresponding ligand orbital. In these circumstances it is clearly an exaggeration to assign half the value of the overlap population to the metal function. This limitation of the Mulliken analysis has been noticed many times in the literature. Dahl and Ballhausen (*37*) discussed, in particular, the problem of the $4s$ and $4p$ AO's in transition-metal complexes and suggested that the overlap population involving these diffuse functions could be assigned entirely to the ligands. Many other alternatives based on a large variety of criteria can be found in review articles by Smith (*38*) and Streitwieser *et al.* (*39*). It appears that all these analyses contain arbitrary criteria and in this sense they should not be considered as conceptual solutions of this problem.[1]

In our case, the alternative proposed by Dahl and Ballhausen (*37*) gives rise to slightly larger $2s$–$4s$ and $2s$–$4p$ charge transfers and noticeably smaller $2p\sigma$–M and $2p\pi$–M transfers. The resulting electronic charges assigned to the nominally empty $4s$ and $4p$ AO's are about 60% of the Mulliken values at 3.99 Bohr and a little greater at larger distances. Such smaller charge transfers give a positive chromium ion with $q_M = 0.22$ a.u. at 4.39 Bohr. Then, $q_L = -0.87$ a.u., and $\alpha = 6.41$. This α should be compared with the Mulliken value, 7.389, in the last row of Table VI. We see that the recipe proposed by Dahl and Ballhausen produces more acceptable values for the ligand–metal charge transfer but the qualitative conclusion deduced from Mulliken analysis still holds: the point-charge cluster deduced either from Mulliken or Dahl and Ballhausen recipe is much more repulsive than the nominal one.

All these results shown that the diffuse functions have in the present calculation a double action. On the one hand, they play a very significant role in obtaining an energy minimum in the nuclear potential of the $^6A_{1g}$ ground state and a negative nonclassical bonding energy, becoming important components in the prediction of a stable ground state for the $(CrF_6)^{5-}$ cluster. On the other hand, the relocalization of electronic charge deduced from the population analysis of the wave function containing these diffuse AO's gives rise to large L–M charge transfers and a classically repulsive cluster.

In addition to the anomalous response on the part of the Mulliken analysis, noticeably attenuated if the recipe proposed by Dahl and Ballhausen (*37*) is followed, one can argue that the L–M transfer deducible from SCF calculations works in this case as a destabilizing mechanism for the cluster, *no matter how large the charge transfer would be*. This can be seen as follows.

Within the L–M transfer, the metallic charge becomes $q_M = -5 - 6q_L$, because the total charge of the cluster (-5 a.u.) is conserved. Then, the constant α can be written as:

$$\alpha = -30q_L + (6 \cdot (2)^{1/2} - 69/2)q_L^2. \quad (3)$$

This equation shows that when q_L goes from the nominal value -1 to less negative values as a consequence of the L–M transfer, α increases. Furthermore, the L–M transfer modifies the energy at infinite separation, $E(\infty)$. The basis sets used in this work give the following energies for the isolated ions:

[1] The molecular structure theory of Bader (*40*) is an example of nonarbitrary analysis of the wave function.

$$E(\mathrm{F};\, q_L) = -11.6979 - 4.03523(5 - q_L) + 0.352856(5 - q_L)^2 \quad (4)$$

$$E(\mathrm{Cr};\, q_M) = -85.5189 - 0.100167q_M + 0.141018q_M^2 + 0.025440q_M^3$$

$$E(\infty) = 6E(\mathrm{F};\, q_L) + E(\mathrm{Cr};\, q_M).$$

The resulting $E(\infty)$ turns out to be a decreasing function of the transferred charge. In consequence, this mechanism modifies the classical intracluster energy by reducing its asymptotic values at $R = \infty$, $E(\infty)$, and increasing its slope α. Thus, neither the large L–M transfer predicted by Mulliken analysis nor the smaller one obtained with the criterion of Dahl and Ballhausen (*37*) would make the nominal cluster more stable. For that reason it could be interesting to explore alternative mechanisms for analyzing the charge redistribution and stability gained in the formation of the Cr^+–F^- bond. We examine this question below.

To conclude this section we will briefly comment on the parameters of ligand spin density $f_i (i = \sigma$ and $\pi)$ derived from the anisotropic coupling constant appearing in the transferred hyperfine interactions. The difference $f_p = f_\sigma - f_\pi$ was reported by Hall *et al.* (*1*) for the Cr^+ : NaF (−0.6%) and Cr^+ : $KMgF_3$ (−1.5%) systems. These numbers have been difficult to interpret theoretically since f_σ is usually larger than f_π in most SCF calculations. For instance, Clack *et al.* (*15*) reported CNDO values obtained with two different basis sets: f_p = 0.55 and 1.13% for Burns and Gouterman bases, respectively. In both calculations f_σ is much larger than f_π. Clack and Monshi (*16*) added INDO values obtained at R = 2.31 Å, the distance corresponding to the NaF host. They are f_σ = 0.74%, f_π = 0.05%, and f_p = 0.69%. Larsson (*17*) argued correctly that the theoretical f_i will be rather basis dependent in any LCAO calculation. His multiple scattering $X\alpha$ calculations include the $(CrF_6)^{5-}$ system for which he finds $f_\sigma = -0.1\%$ and $f_\pi = 0.5\%$, obtaining a very good agreement with the Cr^+ : NaF data. It is interesting to recall that Larsson includes in the calculation of f_σ the contribution of the mainly $4s_M$ a_{1g} MO ($4a_{1g}$ in this work), giving $f_\sigma(a_{1g}) = -0.5\%$ and $f_\sigma(e_g) = 0.4\%$. Further contributions from the mainly $4p_M$ t_{1u} MO might alter the final value.

The spin-density parameters obtained from the present calculation are immediately deducible from the SCF coefficients in Table VI. Near R = 2.31 Å (4.39 Bohr) we find f_σ = 2.37%, f_π = 0.38%, and f_p = 1.89%, values resembling those of Ref. (*15*) although uniformly larger. At smaller distances all these numbers increase. For instance, at R = 1.99 Å ($KMgF_3$) we find, by interpolation, f_σ = 3.8%, f_π = 1.3%, and f_p = 2.5%. Consideration of the a_{1g} and t_{1u} contributions will not make f_p negative since the σ contribution is systematically larger. Perhaps the quality of the present calculation is not enough to describe the ligand density parameters adequately. We would like to recall, however, that the experimental f_i's have been derived making use of the equilibrium distance of the host lattice and neglecting the overlap or two-center contributions in the expectation values of the interaction Hamiltonian. The first approximation could be a serious source of error if, as expected (*14*), noticeable ligand relaxation take place upon cationic substitution in systems like Cr^+ : $KMgF_3$, particularly through the R^{-5} dipolar term. The second approximation has been scarcely studied but it could be comparable to the dipolar term (*30*).

IV. Ligand-to-Lattice (LLAT) Charge Transfer

Let us now examine the symmetric electronic charge transfer from the fluoride ions to the surrounding lattice. In the LLAT mechanism considered here the nominal charge of the cation is unchanged and the

six ligand ions make the same contribution. This charge transfer has the following general characteristics:

(a) It reduces the ligand–ligand repulsion more than the metal–ligand attraction making the nominal cluster more stable.

(b) It gives rise to electron-deficient clusters. It seems interesting to study the electronic structure of these units and, in particular, to know whether they have stable states or not.

(c) It does alter the electronic structure of the next-nearest neighbors of the central metal, modifying the lattice potential and the effects of the cluster–lattice interaction on the reference cluster.

In order to study this transfer, it would be interesting to examine first the LLAT mechanism from a classical-electrostatics point of view. Afterward, we will discuss the SCF results on a quantum electronic state belonging to a particular electron-deficient system.

In the classical-electrostatics LLAT description we have, for the electron-deficient $(CrF_6)^{z-}$ unit, a constant $q_M = +1$ and a varying $q_L = -(z + 1)/6$. In contrast with the L–M mechanism, the total charge of the cluster is not conserved here. Considering z and q_L as independent variables we have

$q_M = -z - 6q_L$, and:

$$\alpha = -6zq_L + (6 \cdot (2)^{1/2} - 69/2)q_L^2. \quad (5)$$

We can consider electron-deficient clusters with $z = 4$ to 0 obtained by LLAT transfers of 1 to 5 electrons. Each of these units has a classical energy determined by the corresponding value of α.

We have plotted in Fig. 3 a family of curves $\alpha(q_L)$, Eq. (5), for $z = 0$ to 5. We can observe that α is positive in the $(CrF_6)^{5-}$ unit for $-1 \leq q_L \leq 0$. The LLAT charge transfer reduces α, producing ranges of negative α's for the electron-deficient clusters. The neutral unit CrF_6 shows a negative α for $-1 \leq q_L \leq 0$. This plot clearly

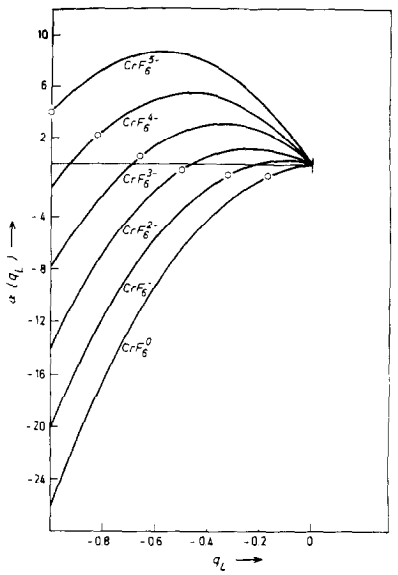

FIG. 3. $\alpha(q_L)$ function, Eq. (5), for the $(CrF_6)^{5-}$ system and five electron-deficient clusters.

shows that the LLAT transfer gives rise to classically less repulsive clusters. We can also observe that for a given unit α increases when q_L becomes less negative than -1, a characteristic of the L–M transfer discussed above.

In Fig. 3 we have marked in each $\alpha(q_L)$ curve the points corresponding to the LLAT transfer considered here, i.e., $q_M = 1$ and $q_L = -(z + 1)/6$. The total charge of the cluster gives the electron deficiency, the value of q_L, and α. For instance, in the neutral CrF_6 unit the deficiency of five electrons gives $q_L = -1/6$ and $\alpha = -0.7226$. This is the point marked in the CrF_6 line in the figure. We observe that the $(CrF_6)^{z-}$ clusters are classically repulsive for $z = 5$, 4, and 3 and attractive for $z = 2$, 1, and 0.

We turn now to the quantum-mechanical analysis. Among the five electron-deficient clusters presented in Fig. 3 we will discuss only the neutral one. This species can be viewed not only as a result of a five-electron LLAT transfer from the $(CrF_6)^{5-}$ system but also as an alternative representa-

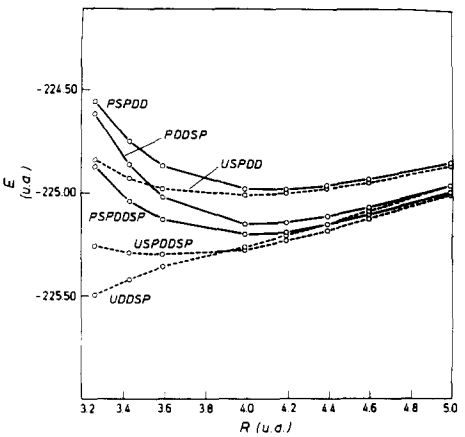

FIG. 4. Potential energy curves for the $^7T_{1u}$ state of the electron-deficient CrF_6 unit.

tion of the cluster-*in-vacuo* model for a Cr^+ center in fluoride lattices. If we accept that each fluoride ion belongs to six clusters, its nominal charge would be $-1/6$ for a given cluster.

In the molecular-orbital study of this unit we first notice that the five electrons can be removed from the $(CrF_6)^{5-}$ cluster in many different ways. We have chosen a transfer from the $2p\pi$ ligand orbitals of the t_{1u} symmetry. These MO's have the highest orbital energies among the occupied set, as can be seen in Table II. We will discuss here the $t_{1u}(^2T_{1u})e_g^2t_{2g}^3(^6A_{1g}) - {}^7T_{1u}$ electronic state.

This state is stable according to the nuclear potential calculations performed with several core-valence partitions. We plot in Fig. 4 the SCF results and the classical energy for this state. As in the $(CrF_6)^{5-}$ unit, the U-DDSP calculation does not give minimum. However, the SPDD description gives minimum in both U and P calculations. Partition and projection effects are similar to those discussed above for the $(CrF_6)^{5-}$ unit and we will not discuss them any longer. From these nuclear potentials we find R_e(P-SPDD) = 2.160 Å, R_e(P-DDSP) = 2.138 Å, and R_e(P-SPDDSP) = 2.100 Å. The neutral species turns out to have an equilibrium distance some 0.24 Å smaller than the 2.375 Å found for the $(CrF_6)^{5-}$ ion. As expected, the LLAT charge transfer reduces the size of the isolated cluster. Notice also, from Fig. 4, that the nonclassical energy of the neutral species is negative for any core-valence partition.

It is interesting to compare the energy of the $^7T_{1u}$ state with the values obtained for other clusters having less electrons than the $(CrF_6)^{5-}$. The $(CrF_6)^{z-}$ systems, with $q_L = -1$ and $q_M = 6 - z = 2$ and 3, for instance, can be considered as electron-deficient units with respect to the $(CrF_6)^{5-}$ system. In these systems the deficiency corresponds nominally to the metal.

In Fig. 5 we have collected the nuclear potential of the $^7T_{1u}$ state and those corresponding to the nominal $(CrF_6)^{z-}$ (z = 5, 4, 3) units. We can observe the different response of the isolated $(CrF_6)^{5-}$ cluster to the different ways of losing electrons. In the region near $R_e((CrF_6)^{5-})$, removal of five electrons from the fluorides reduces the energy of the $^6A_{1g}$ state by about 38 eV. The oxidation of Cr^+ to Cr^{2+} gives the ^5E_g ground state of the $(CrF_6)^{4-}$ cluster some 30

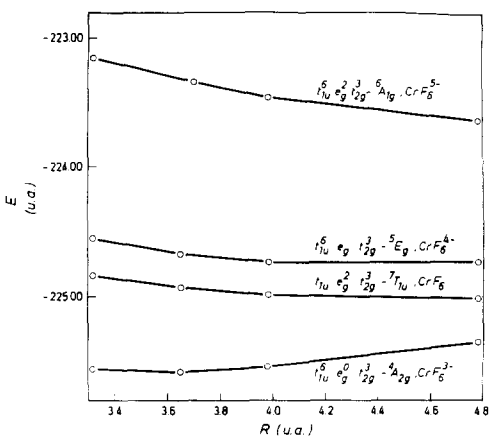

FIG. 5. Nuclear potential of the $^7T_{1u}$ state compared with the ground states of three $(CrF_6)^{z-}$ systems (z = 3–5).

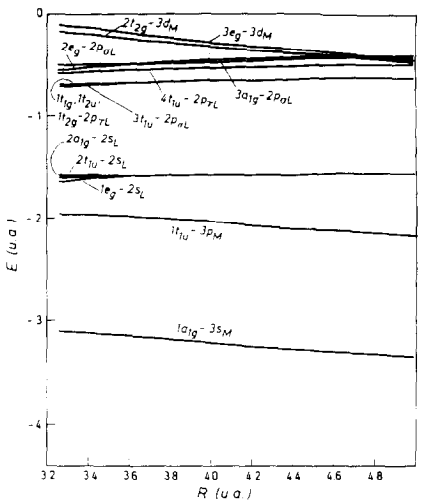

FIG. 6. Orbital energies of the valence MO's computed with the SCF solutions of the $^7T_{1u}$ state of the CrF_6 unit.

eV below the $^6A_{1g}$ state. Further oxidation to Cr^{3+} gives the $^4A_{1g}$ ground state of the $(CrF_6)^{3-}$ system some 50 eV below the $^6A_{1g}$ state.

The LLAT charge transfer produces noticeable changes in the orbital energies of the valence MO's. In Fig. 6 we present these energies, as functions of R, computed with the SCF solutions of the $^7T_{1u}$ state of the neutral CrF_6 unit. This information should be compared with the values for the $(CrF_6)^{5-}$ system in Table II. All the energies are now negative, including those of the antibonding $3e_g$ and $2t_{2g}$ MO's. The LLAT transfer produces a stabilizing effect in the orbital energies analogous to that induced by the cluster–lattice interaction. The $\sigma-\pi$ splitting of the $2p_F$ MO's is greater than that found in the $(CrF_6)^{5-}$ cluster. The $2p_F$ energies lie above and very close to the $3d$ values. All these results reflect a stronger metal–ligand interaction, in agreement with the shape of the nuclear potential of the $^7T_{1g}$ state.

We can now compare the orbital mixing deduced from the septet state with that discussed above from the $^6A_{1g}$ state. The P-SPDDSP SCF coefficients of the mainly metal MO's are collected in Table VII. We observe a general increase in the metal–ligand mixing in agreement with the general view, derived from the curvature of the nuclear potential and the behavior of the orbital energies, of a stronger metal–ligand interaction in the neutral species.

In Table VIII we present the Mulliken population analysis and the metal and li-

TABLE VII

SCF COEFFICIENTS OF THE MAINLY METAL MO'S OBTAINED FROM THE $^7T_{1u}$ STATE OF THE NEUTRAL CrF_6 CLUSTER AT R = 4.59 Bohr

MO	Occup.	$3s_M$	$4s_M$	χ_s	χ_σ	
$4a_{1g}(4s_M)$	0	−0.00479	−1.10868	0.46686	0.60692	
		$3p_M$	$4p_M$	χ_s	χ_σ	χ_π
$5t_{1u}(4p_M)$	0	0.01566	−1.16202	0.53134	0.41999	0.27219
		$3d_M$	$3d_i$	χ_s	χ_σ	
$3e_g(3d_\epsilon)$	2	1.01152	0.00578	−0.20578	−0.36907	
		$3d_M$	$3d_i$	χ_π		
$2t_{2g}(3d_t)$	3	1.05502	−0.06787	−0.17030		

TABLE VIII

ORBITAL POPULATIONS AND METAL AND LIGAND CHARGES ACCORDING TO MULLIKEN POPULATION ANALYSIS ON THE $^7T_{1u}$ STATE OF THE CrF_6 UNIT: P-SPDDSP CALCULATION

	R (Bohr)				
AO	3.99	4.19	4.39	4.59	4.99
$3s_M$	2.000	2.000	1.999	1.999	1.999
$4s_M$	0.357	0.357	0.349	0.335	0.289
$3p_M$	5.984	5.985	5.985	5.985	5.986
$4p_M$	0.268	0.230	0.198	0.172	0.130
$3d_e$	2.199	2.176	2.151	2.126	2.081
$3d_t$	3.058	3.039	3.026	3.017	3.007
$3d$ (total)	5.257	5.215	5.177	5.143	5.088
$2s_F$	1.993	1.995	1.997	1.997	1.998
$2p_F$	5.030	5.041	5.052	5.064	5.087
q(Cr)	0.134	0.214	0.291	0.366	0.510
q(F)	−0.022	−0.036	−0.049	−0.061	−0.085
α	−0.013	−0.033	−0.061	−0.097	−0.188

gand charges deduced from it. Again, these numbers should be compared with those corresponding to the $^6A_{1g}$ state in Table VI. We see that the $3s_M$, $3p_M$, and $4s_M$ MO's present nearly the same occupation as that in the $(CrF_6)^{5-}$ system. The noticeable change appears in the occupation of the $4p_M$ MO. Now the L–M charge transfer is about one-third of the value in Table VI. The reason for that is simply the smaller occupation of the $2p$ orbitals in the neutral species. In contrast, the $F^- \rightarrow 3d$ transfer is slightly larger in the neutral unit. This weaker L–M transfer gives rise to a positive chromium ion, with $q_M = 0.2$ near R_e. The L–M transfer still increases the constant from the nominal $\alpha = -0.7226$, but the resulting values (last row in Table VIII) are negative. Thus, we still have an attractive cluster in spite of the exaggerate L–M transfer derived from Mulliken analysis. Smaller L–M transfers to the diffuse functions and more attractive (α more negative) clusters are found when one uses the partition of the overlap population suggested by Dahl and Balhausen (*37*).

In conclusion, we observe that the LLAT mechanism can give rise to electron-deficient clusters that

(a) are classically attractive units,
(b) are smaller than the nominal $(CrF_6)^{5-}$ system, and
(c) have stable electronic states.

Furthermore, the metal–ligand mixing and covalency are exalted by the LLAT transfer. The MO's have smaller orbital energies and the splitting of the $2p_F$ states increases. Thus, this mechanism gives rise to electron-deficient units more stable and with stronger metal–ligand bonding interaction than the nominal $(CrF_6)^{5-}$ cluster. It could be an interesting approach to deal with highly charged clusters, such as those corresponding to monopositive centers.

The above properties have been deduced from the electronic structure of the neutral CrF_6 unit *in vacuo*. To complete the comparison with the $(CrF_6)^{5-}$ cluster we should incorporate this unit in the lattice of the NaF. We have performed a cluster-in-lattice calculation based on the point-charge

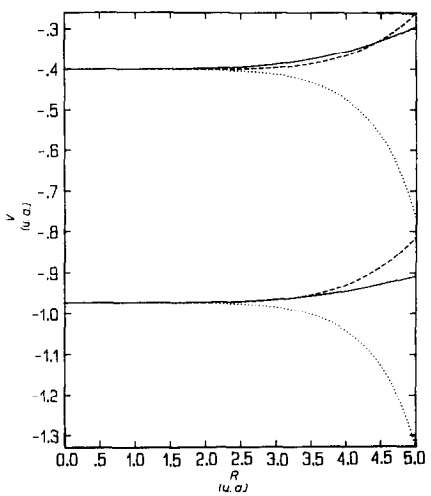

FIG. 7. Ewald lattice potential along the 100 (solid lines), 110 (dotted lines), and 111 (broken lines) directions for the regular NaF (lower plot) and the electron-rich NaF (upper plot).

lattice model described above. The five electrons transferred from the chromium cluster have been accommodated isotropically in the six first neighbor ions along the 100 direction. Each of these sodium ions receives 5/6 of electron from the chromium cluster and becomes a point charge of value +1/6 a.u. in our lattice model. Admittedly, this mechanism is quite artificial because it claims a highly directed charge transfer and assumes that the Na^+ ions are able to receive electrons from the fluoride neighbors. Nevertheless, it takes care of the balance of electrons and appears to be consistent with the point-charge lattice model described above.

This electron-rich lattice produces a lattice potential in the volume of the chromium cluster noticeably smaller than that of the regular lattice. In Fig. 7 we present the Ewald results (*36*) along the 100, 110, and 111 directions for the regular and the electron-rich NaF. These values are negative because they are expressed as potential energy of an electron. From this plot we can anticipate that the lattice effects of the electron-rich NaF would be much smaller than those of the regular crystal.

In Table IX we collect the valence energy of the neutral CrF_6 unit *in vacuo* and inside the potential of the electron-rich NaF. These entries can be compared with those in Table III corresponding to the $(CrF_6)^{5-}$ cluster and the regular NaF. As expected, the neutral unit suffers a negligible stabilization (smaller than 1 eV) in the field of the electron-rich NaF. Now we can see that whereas the neutral unit *in vacuo* has a valence energy some 38 eV below the value of the $(CrF_6)^{5-}$ cluster *in vacuo*, the lattice effects reverse the situation making the pentanegative species in the lattice more stable than the neutral species in the electron-rich lattice. This means that the LLAT transfer is not an stabilizing mechanism inside the lattice. Furthermore, the reduction of the equilibrium distance for the neutral unit in the lattice is 0.02 Å versus 0.18 Å for the pentanegative cluster.

TABLE IX

P-SPDDSP VALENCE ENERGIES (HARTREE), PLUS 224 HARTREES, OF THE ELECTRON-DEFICIENT CrF_6 UNIT *in Vacuo* AND EMBEDDED IN THE POINT-CHARGE POTENTIAL OF THE ELECTRON-RICH NaF

	R (Bohr)					
	3.59	3.99	4.19	4.39	4.59	4.99
In vacuo	−1.13156	−1.20265	−1.18667	−1.15240	−1.10606	−0.99437
In NaF	−1.14527	−1.20882	−1.18217	−1.13141	−1.06170	−0.86986

It appears that the electronic structure of the electron-deficient cluster generated by the LLAT mechanism is nearly independent of the lattice effects (within the model used here), as it corresponds to a neutral object that, in addition, is located in a lattice potential much smaller than the regular one. This gives further interest to the properties deduced from the cluster-*in-vacuo* analysis of this unit and confirms that it represents a possible model for approximate cluster-*in-vacuo* descriptions of monopositive centers. This conclusion is not in contradiction with the general view deduced from this and related works (*14, 18, 19*) that a deep understanding of the physical properties of monopositive $3d$ ions in crystal lattices would require elaborate theoretical analysis based on large clusters and rigorous lattice models. Since this type of analysis is difficult and expensive, it still seems reasonable to explore alternative approximate models, such as those discussed in this paper.

Acknowledgment

Financial support from CAICYT under Project No. 2880/83 is gratefully acknowledged.

References

1. T. P. P. Hall, W. Hayes, R. W. H. Stevenson, and J. Wilkens, *J. Chem. Phys.* **38,** 1977 (1963).
2. J. J. Davies and K. Horai, *J. Phys. C* **4,** 671, 682 (1971).
3. H. Ziegler, *Phys. Status Solidi B* **49,** 367 (1972).
4. H. L. Van Camp and Y. W. Kim, *Phys. Rev. B* **11,** 3098 (1975).
5. R. Alcalá, P. J. Alonso, V. M. Orera, and H. W. den Hartog, *Phys. Rev. B* **32,** 4158 (1985).
6. V. M. Orera, R. Alcalá, and P. J. Alonso, *Solid State Commun.* **58,** 79 (1986).
7. R. Cases, P. J. Alonso, R. Alcalá, and J. M. Spaeth, *Cryst. Lattice Defects Amorphous Mater.* **16,** 289 (1987).
8. T. L. Estle and W. C. Holton, *Phys. Rev.* **150,** 159 (1966).
9. J. J. Davies, *Phys. Lett. A* **40,** 423 (1972).
10. E. Simánek and K. A. Müller, *J. Phys. Chem. Solids* **31,** 1027 (1970).
11. A. M. Hennel and G. Martínez, *Phys. Rev. B* **25,** 1039 (1982).
12. M. Moreno, J. Aramburu, and M. T. Barriuso, *Phys. Lett. A* **87,** 307 (1982).
13. M. T. Barriuso and M. Moreno, *Phys. Rev. B* **29,** 3623 (1984).
14. G. Fernández Rodrigo, L. Pueyo, M. Moreno, and M. T. Barriuso, *J. Solid State Chem.* **67,** 64 (1987).
15. D. W. Clack, N. S. Hush, and J. R. Yandle, *J. Chem. Phys.* **57,** 3503 (1972).
16. D. W. Clack and M. Monshi, *Rev. Roum. Chim.* **23,** 495 (1976).
17. S. Larsson, *Phys. Lett. A* **45,** 185 (1973).
18. V. Luaña, G. Fernández Rodrigo, E. Francisco, L. Pueyo, and M. Bermejo, *J. Solid State Chem.* **66,** 263 (1987).
19. V. Luaña, G. Fernández Rodrigo, M. Flórez, E. Francisco, J. M. Recio, J. F. Van der Maelen, L. Pueyo, and M. Bermejo, *Cryst. Lattice Defects Amorphous Mater.* **15,** 19 (1987).
20. G. Fernández Rodrigo, Thesis Dissertation, Universidad de Oviedo (1986).
21. J. W. Richardson, T. F. Soules, D. M. Vaught, and R. R. Powell, *Phys. Rev. B* **4,** 1721 (1971).
22. J. W. Richardson, W. C. Nieuwpoort, R. R. Powell, and W. F. Edgell, *J. Chem. Phys.* **36,** 1057 (1962).
23. J. W. Richardson, R. R. Powell, and W. C. Nieuwpoort, *J. Chem. Phys.* **38,** 796 (1963).
24. T. F. Soules, J. W. Richardson, and D. M. Vaught, *Phys. Rev. B* **3,** 2186 (1971).
25. L. Pueyo and J. W. Richardson, *J. Chem. Phys.* **67,** 3584 (1977).
26. L. Seijo, L. Pueyo, and F. Gómez Beltrán, *J. Solid State Chem.* **42,** 28 (1982).
27. S. Gutiérrez Orellana and L. Pueyo, *J. Solid State Chem.* **55,** 30 (1984).
28. M. Flórez, L. Seijo, and L. Pueyo, *Phys. Rev. B* **34,** 1200 (1986).
29. B. L. Kalman and J. W. Richardson, *J. Chem. Phys.* **55,** 4443 (1971).
30. T. F. Soules and J. W. Richardson, *Phys. Rev. Lett.* **25,** 110 (1970).
31. Z. Barandiarán and L. Pueyo, *J. Chem. Phys.* **79,** 1926 (1983); **80,** 1597 (1984).
32. S. Huzinaga and A. A. Cantú, *J. Chem. Phys.* **55,** 5543 (1971).
33. V. Bonifacic and S. Huzinaga, *J. Chem. Phys.* **60,** 2779 (1974): **62,** 1509 (1975).
34. S. Sakai and S. Huzinaga, *J. Chem. Phys.* **76,** 2552 (1982).

35. L. Seijo, Z. Barandiarán, V. Luaña, and L. Pueyo, *J. Solid State Chem.* **61,** 269 (1986).

36. A. G. Piken and W. van Gool, Ford Technical Report No. SL 68-10 (1968).

37. J. P. Dahl and C. J. Ballhausen, *Adv. Quantum Chem.* **4,** 170 (1968).

38. V. H. Smith, Jr., *Phys. Scr.* **15,** 147 (1977).

39. A. Streitwieser, Jr., J. B. Collins, J. M. McKelvey, D. Grier, J. ender, and A. G. Toczko, *Proc. Natl. Acad. Sci. USA* **76,** 2449 (1979).

40. R. F. W. Bader and T. T. Nguyen-Dang, *Adv. Quantum Chem.* **14,** 63 (1981).